BeBeC-2020-D02

APPLICATION OF THE CLEANT METHOD FOR HIGH SPEED RAILWAY TRAIN MEASUREMENTS

Adam Kujawski and Ennes Sarradj
TU Berlin, FG Technische Akustik
Einsteinufer 25, 10587 Berlin, Germany

Abstract

Localization and quantification of noise emitted by trains with a microphone array can be a challenging task, particularly when a train is moving at high speed. The microphone array is often placed close to the observation plane which results in a pronounced Doppler frequency shift over time. The application of conventional beamforming in the time domain leads to unsatisfactory results due to highly limited spatial resolution of the resulting sound maps, especially at low frequencies. In order to overcome those limitations, existing deconvolution methods were adapted to moving source scenarios. However, these methods are all performed in the frequency domain. Recently, the CLEANT method has been proposed that performs a deconvolution exclusively in the time domain. The authors showed that this method leads to more accurate results for the localization and quantification of moving sources than previously used methods.
In this contribution, the CLEANT algorithm is applied on microphone array data from high speed railway train measurements with 96 sensors. Two vehicles driving with constant speeds of 275 km/h and 278 km/h are analyzed. The method provides source maps with improved spatial resolution.

1 INTRODUCTION

High speed railway trains are of major importance for the public passenger transport in modern industrial countries. They offer the advantage of fast and energy efficient transportation with small carbon footprint compared to air or car traffic. However, acceptance among the population is hampered by the noise pollution in the vicinity of railway tracks caused by moving trains. Typically, noise mitigation measures, such as noise barriers, are used to reduce the noise level in particularly affected areas. Nevertheless, reducing sound generation itself can be a more favourable noise control measure since it has no environmental impact. This requires an accurate identification and quantification of the noise sources.
In order to characterize the noise sources of a railway train under certain operating conditions, the application of beamforming has been a common tool for decades [1, 6, 8, 11]. Depending on the driving speed, different noise mechanisms like aerodynamic noise and rolling noise can be observed by this method [10]. Aerodynamic noise is caused by air flow over the train body structure, whereas rolling noise is caused by the wheel-rail interaction. Control of aerodynamic source mechanisms at high-speed trains is of particular interest since their sound power scales more rapidly with flow speed.
Microphone array measurements can be performed under isolated conditions, like in wind tunnels [11]. Wind tunnel measurements allow arbitrarily long acquisition durations and enable testing and controlling a variety of constructional and experimental parameters without the presence of engine or rolling noise. However, only aerodynamic sources can be characterized in such analysis. In contrast, array measurements in a real environment are also common, whereby the train passes by an arrangement of microphones positioned alongside the railway track [1]. Pass-by measurements are of importance in order to analyze the noise level of a vehicle under operating conditions.
The analysis of collected array data from a vehicle pass-by can be challenging when the train is moving at high-speed. A Doppler frequency shift affects the channel data, especially when the array is placed close to the railway track. This influence can be eliminated when the beamforming method is applied in the time domain and the array focus is moved along the sources trajectory [2]. However, deconvolution techniques that improve the spatial resolution of beamformed sound maps are commonly used in the frequency domain. Thus, frequency-based deconvolution methods had to be adapted in order to account for moving source scenarios but are only suitable under certain conditions [5]. Cousson et al. [3] recently proposed the CLEANT method which performs a deconvolution exclusively in the time domain. In this contribution, it is shown that the application of this method to microphone array data from high-speed train measurements can lead to promising results regarding spatial resolution and quantification of sound sources compared to the standard delay-and-sum method.

2 MICROPHONE ARRAY METHODS FOR MOVING SOURCES

Beamforming can be performed in time or frequency domain. When evaluated in the time domain, the method is commonly called delay-and-sum beamforming, due to its simple principle of summing a set of individually delayed sound pressure signals $\{p_m\}$ of N sensors. The

delay-and-sum method determines the radiated sound pressure

$$b(t,\mathbf{x}_\mathrm{g},\{p_m\}) = \frac{1}{K_{\mathbf{x}_\mathrm{g}}(t)} \sum_{m=1}^{N} w_m \frac{p_m(t+\frac{r_{\mathbf{x}_\mathrm{g}m}(t)}{c})}{r_{\mathbf{x}_\mathrm{g}m}(t)(1-M\cos\theta_{\mathbf{x}_\mathrm{g}m}(t))^2},$$
$$K_{\mathbf{x}_\mathrm{g}}(t) = \sum_{m=1}^{N} \frac{w_m}{\left[r_{\mathbf{x}_\mathrm{g}m}(t)(1-M\cos\theta_{\mathbf{x}_\mathrm{g}m}(t))^2\right]^2}, \tag{1}$$

emitted by an assumed monopole source located at a focus point $\mathbf{x}_\mathrm{g}$ at time t. In eq. 1, c is the speed of sound, w_m is the spatial weighting coefficient of the m-th microphone and $K_{\mathbf{x}_\mathrm{g}}$ is the normalization term. The trajectory of a moving monopole source is usually followed by changing the position of the focus point over time. Therefore, the distance between the steered location and the respective m-th sensor, $r_{\mathbf{x}_\mathrm{g}m}(t)$, becomes time-dependent. As a result, the Doppler frequency shift can be removed [2]. In order to additionally take the motion-induced convective amplification into account, the received sound pressure $p_m(t)$ is weighted by $1/(1-M\cos\theta_{\mathbf{x}_\mathrm{g}m}(t))^2$, whereby M is the Mach number and $\theta_{\mathbf{x}_\mathrm{g}m}(t)$ the time-dependent angle between the moving source and the corresponding sensor direction. The squared sound pressure emitted by the source at the focus point $\mathbf{x}_\mathrm{g}$ is then $b_\mathrm{Sq}(t,\mathbf{x}_\mathrm{g}) = [b(t,\mathbf{x}_\mathrm{g},\{p_m\})]^2$.

For the frequency domain beamforming method, techniques already exist to minimize the influence of uncorrelated self-noise at the array sensors [4]. Widely adapted is the method of removing the main diagonal of the cross-spectral matrix (CSM) [12]. A similar diagonal deletion technique has been proposed for the delay-and-sum method by Dougherty [4]. Hereby, the auto-power is removed from the squared beamforming result $b_\mathrm{Sq}(t,\mathbf{x}_\mathrm{g})$, which yields the squared beamforming result with diagonal deletion

$$b_\mathrm{Sq,R}(t,\mathbf{x}_\mathrm{g}) = b_\mathrm{Sq}(t,\mathbf{x}_\mathrm{g}) - \sum_{m=1}^{N} \left[\frac{w_m}{K_{\mathbf{x}_\mathrm{g}}(t)} \frac{p_m(t+\frac{r_{\mathbf{x}_\mathrm{g}m}(t)}{c})}{r_{\mathbf{x}_\mathrm{g}m}(t)(1-M\cos\theta_{\mathbf{x}_\mathrm{g}m}(t))^2}\right]^2. \tag{2}$$

2.1 DECONVOLUTION METHODS

Deconvolution aims to remove the influence of the point-spread function and to recover the initial source constellation on the basis of the beamforming result [3, 5, 7]. In case of moving sources, the common assumption is that the spatial response (point-spread function) of a corresponding microphone array is approximately isotropic. Another frequently made assumption is that the influence of the Doppler frequency shift is small due to a quasi-static behavior of the sources within an evaluated snapshot [5]. This allows the use of deconvolution methods in frequency domain, which is appropriate for the analysis of distant sources like wind turbines and aircrafts [5]. However, this assumption cannot be satisfied in the case of railway pass-by measurements with the array placed close to the track. The CLEANT method proposed by Cousson et al. [3] is exclusively performed in the time domain which allows a dedopplerization [2] by moving the array focus with the source's trajectory.

Essentially, CLEANT aims to iteratively find a clean representation $\Gamma(t,\mathbf{x}_\mathrm{g})$ of the beamforming result $b\left(t,\mathbf{x}_\mathrm{g},\{p_m\}\right)$. First, the initial beamforming result $\Phi^{(0)}(t,\mathbf{x}_\mathrm{g})$, the clean signal $\Gamma^{(0)}(t,\mathbf{x}_\mathrm{g})$

and the residual microphone signals $p_m^{\mathrm{res}(0)}(t)$ are initialized by

$$\begin{aligned} \Phi^{(0)}(t,\mathbf{x}_\mathrm{g}) &= b\left(t,\mathbf{x}_\mathrm{g},\{p_m\}\right), \\ \Gamma^{(0)}(t,\mathbf{x}_\mathrm{g}) &= 0, \\ p_m^{\mathrm{res}(0)}(t) &= p_m(t). \end{aligned} \tag{3}$$

In the second step the strongest source is localized within a defined search grid of sources at the i-th iteration. According to equation 4, the source showing the highest energy content at $\hat{\mathbf{x}}_\mathrm{g}$ is determined by integrating over a time frame T:

$$\hat{\mathbf{x}}_\mathrm{g} = \underset{\mathbf{x}_\mathrm{g}}{\operatorname{argmax}} \left(\int_T \left| \Phi^{(i-1)}(t,\mathbf{x}_\mathrm{g}) \right|^2 dt \right). \tag{4}$$

This signal is subsequently added to the clean representation:

$$\Gamma^{(i)}(t,\hat{\mathbf{x}}_\mathrm{g}) = \Gamma^{(i-1)}(t,\hat{\mathbf{x}}_\mathrm{g}) + \gamma \Phi^{(i-1)}(t,\hat{\mathbf{x}}_\mathrm{g}), \tag{5}$$

where γ defines a loop gain that scales the magnitude of the signal which is added to Γ. The next step consists of modelling the microphone signals caused by this source signal and subtracting them from the residual microphone signals:

$$p_m^{\mathrm{res}(i)}\left(t+\frac{r_{\mathbf{x}_\mathrm{g}m}}{c}\right) = p_m^{\mathrm{res}(i-1)}\left(t+\frac{r_{\mathbf{x}_\mathrm{g}m}}{c}\right) - \gamma \frac{\Phi^{(i-1)}(t,\hat{\mathbf{x}}_\mathrm{g})}{r_{\hat{\mathbf{x}}_\mathrm{g}m}(t)\left(1-M\cos\theta_{\hat{\mathbf{x}}_\mathrm{g}m}(t)\right)^2}. \tag{6}$$

Finally, beamforming is performed again with the residual microphone signals:

$$\Phi^{(i)}(t,\mathbf{x}_\mathrm{g}) = b\left(t,\mathbf{x}_\mathrm{g},\{p_m^{\mathrm{res}(i)}\}\right) \tag{7}$$

The method is performed for a certain number of iterations. According to Cousson et al. [3], the stop criterion is reached when there is an increase of energy within the residual beamforming map $\Phi^{(i)}(t,\mathbf{x}_\mathrm{g})$ or when a maximum number of iterations has been reached.
The final clean signal representation $\Gamma(t,\mathbf{x}_\mathrm{g})$ can be written as the sum of individual components $\Phi^{(k)}(t,\mathbf{x}_\mathrm{g})$ found in a set of iterations $K \subseteq \{1,\cdots I\}$ during a full run of the method consisting of the total of I iterations, so that

$$\Gamma(t,\mathbf{x}_\mathrm{g}) = \gamma \sum_{k\in K} \Phi^{(k)}(t,\mathbf{x}_\mathrm{g}) = \gamma \sum_{k\in K} b\left(t,\mathbf{x}_\mathrm{g},\{p_m^{\mathrm{res}(k)}\}\right). \tag{8}$$

Finding a satisfying clean representation might be challenging in the presence of high channel self-noise, since this noise causes additional maxima in the beamforming map. As already mentioned, one approach to eliminate self-noise induced maxima from the beamforming map is to delete the diagonal containing the auto-correlations of the microphone signals according to eq. 2. The diagonal deletion approach cannot be directly applied here, as the nature of the CLEANT method requires to model the sound pressure signals at the microphones on the basis of the corresponding beamformed source signal. Nevertheless, it is be possible to use the

diagonal deleted result to find the focus point emitting the highest energy, so that eq. 4 becomes

$$\hat{\mathbf{x}}_\mathrm{g} = \underset{\mathbf{x}_\mathrm{g}}{\operatorname{argmax}} \left(\int_T b_{\mathrm{Sq,R}}^{(i-1)}(t, \mathbf{x}_\mathrm{g} \left\{ p_m^{\mathrm{res}(i)} \right\}) dt \right). \tag{9}$$

This step avoids the identification of incorrect source positions that exist due to beamformed self noise, but the additive noise components are still part of the clean map.
If the loop gain value is not low and the scan grid is highly resolved, a source position often is found only once during the deconvolution process and the energy originating from an adjacent grid point is removed in the following iterations. As a result, $\Gamma(t, \mathbf{x}_\mathrm{g})$ in eq. 8 becomes approximately

$$\Gamma(t, \mathbf{x}_\mathrm{g}) \approx \gamma b \left(t, \mathbf{x}_\mathrm{g}, \{ p_m^{\mathrm{res}(k)} \} \right). \tag{10}$$

In this case, the diagonal deletion can be applied analogous to eq. 2 for the CLEANT method:

$$\Gamma_{\mathrm{Sq,R}}(t, \mathbf{x}_\mathrm{g}) = [\Gamma(t, \mathbf{x}_\mathrm{g})]^2 - \gamma^2 \sum_{m=1}^{N} \left[\frac{w_m}{K_{\mathbf{x}_\mathrm{g}}(t)} \frac{p_m^{\mathrm{res}(k)}(t + \frac{r_{\mathbf{x}_\mathrm{g}m}(t)}{c})}{r_{\mathbf{x}_\mathrm{g}m}(t)(1 - M \cos \theta_{\mathbf{x}_\mathrm{g}m}(t))^2} \right]^2. \tag{11}$$

It will be shown later that this step can improve the signal to noise ratio of the deconvolved maps.

3 EXPERIMENTAL DATA

Considered are measurements of two electric multiple-unit trains. Each of the vehicles was measured on one of the two parallel-running railway tracks A and B (Fig. 1). The runs were carried out at a speed of $v_\mathrm{A} = 275\,\mathrm{km/h}$ and $v_\mathrm{B} = 278\,\mathrm{km/h}$ driving in the same direction, but with the pantographs pointing in opposite directions. The sound pressure signals of the individual pass-by runs were acquired with a microphone array consisting of 96 sensors with an aperture size of 4.3 m, placed in the distance $d_\mathrm{A} = 9.17\,\mathrm{m}$ from Track A and $d_\mathrm{B} = 4.49\,\mathrm{m}$ from the Track B. The noise emitted by the individual runs on both tracks was evaluated by applying time domain beamforming and deconvolution via CLEANT method. The setup used for the evaluation is shortly explained in the following.
Only parts of the moving vehicles were evaluated within a predefined monitoring area. A grid that covers the entire area of interest would be unfeasible due to the length of the trains and poor array response at large observation angles. In general, a large monitoring area is advantageous to yield a better approximation of the expectation value of the source strength. However, main-lobe width and side-lobe level of the point-spread function increase with growing incident angle. A moving rectangular grid that consists of the individual focus points representing possible source positions of 4 m width, 6.6 m height and a spacing of $\Delta x = 0.2\,\mathrm{m}$ was determined. The maximum observation angle was set to $\theta = 75^\circ$, which results in a monitoring distance of 14 m for Track A and 6.9 m for Track B. This setting allows qualitatively acceptable characteristics of the point-spread function, even at the maximum observation angle. The vehicle sub-sections evaluated inside the monitoring area were combined at the end. In order to correctly account for the sources that appear at the edges of the focus area, an overlap of 50% was defined. Each

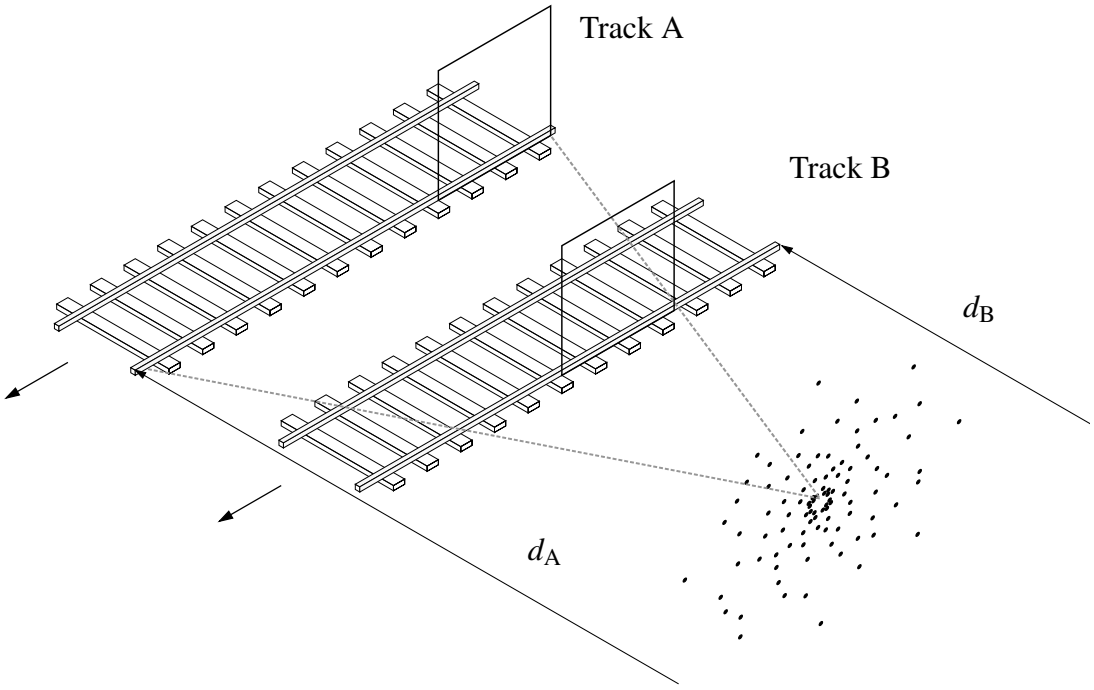

Figure 1: Measurement and analysis setup of the experimental microphone array data. The gray dotted line indicates the observation angle of the array. The black rectangles indicate the focus grid moving inside the covered monitoring area.

Table 1: Properties of the train measurements on Track A and Track B.

Property	Track A	Track B
Distance Array - Rail	$d_A = 9.17\,\mathrm{m}$	$d_B = 4.49\,\mathrm{m}$
Driving Speed	$v_A = 275\,\mathrm{km/h}$	$v_B = 278\,\mathrm{km/h}$
Monitoring Area Length	$14\,\mathrm{m}$	$6.9\,\mathrm{m}$
Focus Grid	$x \in [0\,\mathrm{m}, 4\,\mathrm{m}], y \in [-3\,\mathrm{m}, 3.6\,\mathrm{m}], \Delta x = \Delta y = 0.2\,\mathrm{m}$	
Microphone Array	96 sensors, aperture size $d = 4.3\,\mathrm{m}$	
Block Size	256 samples	
Map Overlap	50 %	
Window	Hanning	
Sampling Rate	$f_s = 32\,\mathrm{kHz}$	

sub-section was weighted by a hanning window. The measurement setup is depicted in Figure 1 and the main properties are summarized in Table 1.

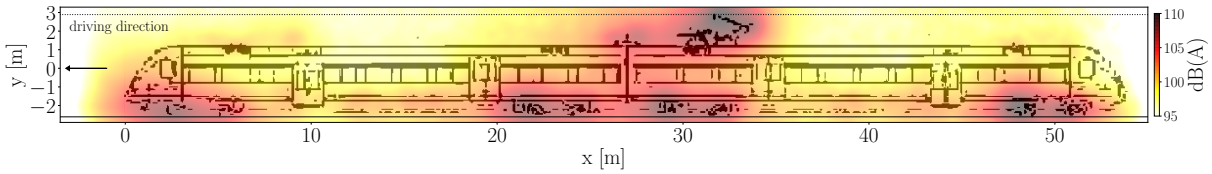

(a)

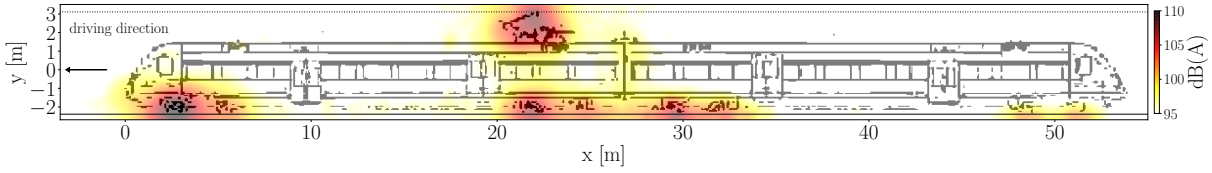

(b)

Figure 2: Source maps obtained by beamforming with diagonal deletion showing the A-weighted sum of third octave bands between 250 Hz *and* 3150 Hz*, collected at Track A (a) and Track B (b).*

4 RESULTS

The beamforming maps in Figure 2 show the sum of the A-weighted third octave bands between 250 Hz and 3150 Hz for each train under investigation. The horizontal dotted line indicates the catenary, whereas the horizontal straight line marks the rail. The calculation of the beamforming result was carried out with diagonal deletion according to eq. 2. Several source regions can be recognized from the given source maps. A large part of the emitted noise can be attributed to the bogies. Especially the leading bogie of the train B has a major impact on the overall-level which is caused not only by the rolling noise but also by the flow noise. Further, the pantograph can be determined as a prominent source region located at the top of the carbody. Weaker aeroacoustic sources might appear but cannot be identified from the given sound maps, as the side-lobe level limits the dynamic range to an acceptable value of 15 dB. It is noticeable that the spatial resolution is poorer for Track A, which is due to the larger distance of the array from the track and the related unfavorable properties of the point-spread function. Another reason for the reduced resolution might be the presence of turbulence caused by wind during the measurement of Train A.

In the following, results achieved by CLEANT deconvolution method are examined. Figure 3(a) and 3(b) show the A-weighted deconvolved source maps between 250 Hz and 3150 Hz yielded by the method for $\gamma = 0.6$, a maximum of 30 iterations per snapshot and without diagonal removal. The main source regions are framed for later spatial integration. Thereby, the four bogies (dashed-dotted frame) and the pantograph area (dashed frame) are treated as two separate source regions.

Regarding the pantograph, a clear improvement of the spatial resolution can be observed for both source maps. For Train A, the panhead and knee joint are the predominant source regions, whereas the panhead can be identified as the area to emit the highest noise levels for Train B.

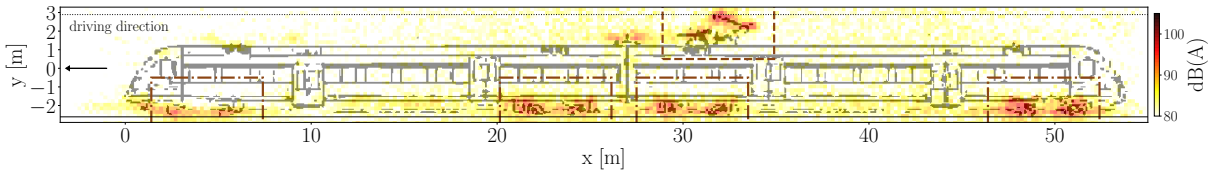

(a)

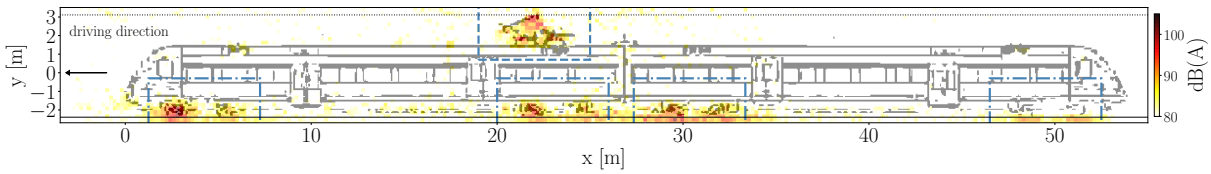

(b)

*Figure 3: Deconvolved source maps without diagonal deletion showing the A-weighted sum over third octave bands between 250 Hz and 3150 Hz, collected at Track A (a) and Track B (b). ($\gamma = 0.6$, **without diagonal deletion**)*

Further sources can be identified at the structures that exceed the recess area in both noise maps. In general, the assignment of levels to the train components is more difficult at Track B, which can be attributed to the shorter observation time leading to fewer averaged snapshots.

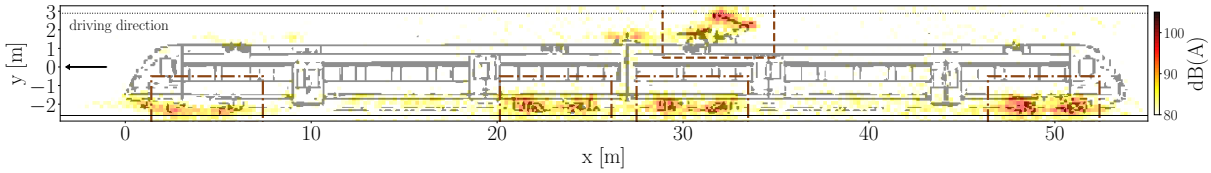

(a)

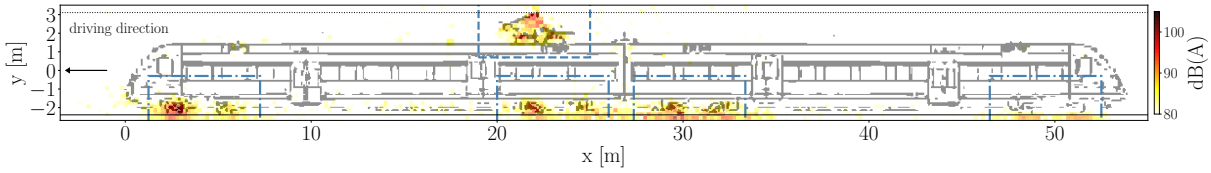

(b)

*Figure 4: Deconvolved source maps examined with the CLEANT method showing the A-weighted sum over third octave bands between 250 Hz and 3150 Hz, collected at Track A (a) and Track B (b). ($\gamma = 0.6$, **with diagonal deletion**)*

An improved spatial resolution can be observed at the bogie regions but with limited extent. A separation of sources that are due to rail-wheel interaction or induced by the flow is not possible from the clean representation, since various source mechanisms interact in close proximity. Especially noticeable is the presence of many weak pseudo-sources that are distributed over a large area of the map and occur in the areas that are not in the immediate vicinity of the train. This is especially true for Train A in Figure 3(a). One reason can be uncorrelated flow or self noise at the sensors. By applying deconvolution with diagonal deletion as introduced in this contribution (see: eq. 11), these artefacts can be significantly reduced. As shown in Figure 4(a) and 4(b), further weaker sources can now be identified, such as at the top end of the intercoaches gap of Train A. Nevertheless, not all of the apparent pseudo sources in the map can be removed by applying diagonal deletion. This is particularly true for the map regions surrounding the existing dominant sources. This may be due to the fact that with the evaluation of noise in a spatially limited sub-area, side-lobes of stronger sources outside appear as additional sources inside the area. As a consequence, these side-lobes are interpreted as true sources in the deconvolution process since their positions are spatially stationary and their power is contained in the microphone signals. Nevertheless, as additionally shown by the individual one-third octave maps for Train A (Figure 6) and Train B (Figure 7), the main sources show a good correspondence with the expected source areas and are highly resolved.
In order to quantify the noise emitted by the individual components, a spatial integration of the deconvolved squared sound pressure values was performed. Figure 5 shows the integrated A-weighted third-octave levels of the bogie sections (dashed-dotted line) and the pantograph (dashed line). The overall level was maintained by integrating the entire train region and is illustrated by a solid line. The one-third octave levels show that the total noise is mainly caused by the sources at the bogies. Comparing the noise levels originating from the pantograph region of both trains, Train A produces slightly higher levels. One explanation may be that the knee joint of Train A points opposite to the direction of travel. Turbulence at the exposed pan head causes additional noise at the rear knee joint. This is further enhanced by various turbulence-generating structures located in front of the pantograph A.

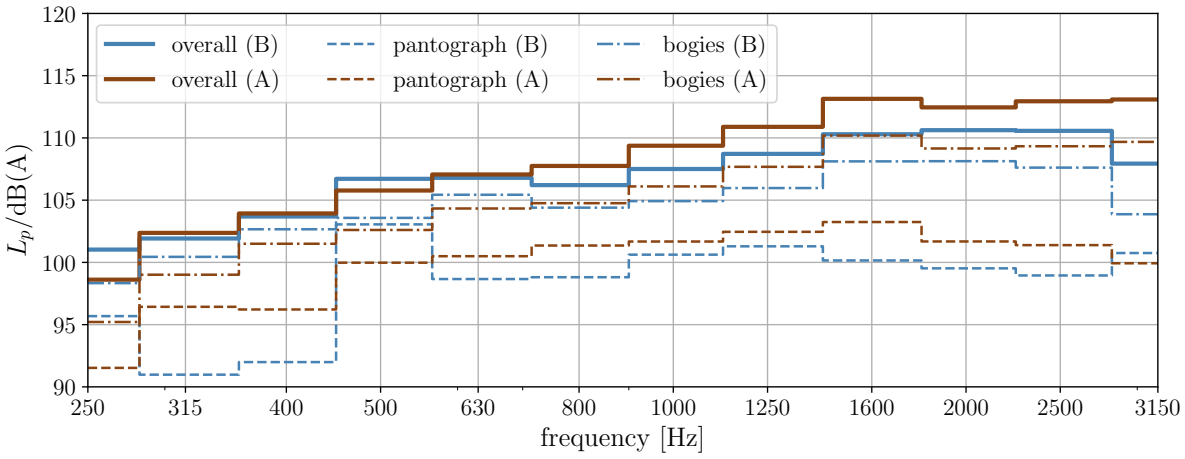

Figure 5: One-third octave levels of the individual components of train A (brown) and train B (blue).

With regard to the validity of the quantification results, it should be noted that the underlying assumption of uncorrelated radiating monopoles does not apply for most of the sources occurring at the train [13]. Apart from the noise radiated from the wheels, highly directional source characteristics are common which leads to inaccurate source strength estimates. However, for directional sources pointing towards the array, this discrepancy has only minor influence when the monitoring area is small [14]. Moreover, Zhang et al [14] showed that with prior knowledge about the source orientation it is possible to use compensation factors to account for the occurring inaccuracy.

5 CONCLUSION

This work has shown that a considerable improvement in the identification of sources at high-speed trains can be achieved by the application of CLEANT deconvolution compared to the beamforming method. In contrast to previous publications using beamforming [9], the deconvolution allows a much more accurate assignment of the sources in the sound maps to their places of origin. Furthermore, the strength of the individual sources can be calculated by integration over a spatial area. This work has also shown that by removing the auto-power of the microphone signals after deconvolution, an additional improvement in terms of signal to noise ratio can be achieved.

REFERENCES

[1] B. Barsikow. "Experiences with various configurations of microphone arrays used to locate sound sources on railway trains operated by the db ag." *Journal of Sound and Vibration*, 193(1), 283–293, 1996. doi:10.1006/jsvi.1996.0269.

[2] B. Barsikow and W. King. "On removing the doppler frequency shift from array measurements of railway noise." *Journal of Sound and Vibration*, 120(1), 190 – 196, 1988. ISSN 0022-460X. doi:https://doi.org/10.1016/0022-460X(88)90344-6. URL `http://www.sciencedirect.com/science/article/pii/0022460X88903446`.

[3] R. Cousson, Q. Leclère, M.-A. Pallas, and M. Berengier. "A time domain clean approach for the identification of acoustic moving sources." *Journal of Sound and Vibration*, 443, 47–62, 2019. doi:10.1016/j.jsv.2018.11.026.

[4] R. P. Dougherty. "Advanced Time-domain Beamforming Techniques." In *10th AIAA/CEAS Aeroacoustics Conference, Manchester, Great Britain, May 10-12, 2004*. 2004.

[5] V. Fleury and J. Bulté. "Extension of deconvolution algorithms for the mapping of moving acoustic sources." *The Journal of the Acoustical Society of America*, 129, 1417–1428, 2011. doi:10.1121/1.3531939.

[6] J. Gomes, J. Hald, and B. Ginn. "Localising noise sources on a rail vehicle during pass-by." In *IWRN13, International Workshop on Railway Noise (2013)*. 2013.

[7] S. Guérin and C. Weckmueller. "Frequency-domain reconstruction of the point-spread function for moving sources." In *Proceedings on CD of the 2nd Berlin Beamforming Conference, 19-20 February, 2008*. 2008.

[8] W. F. King III and D. Bechert. "On the Sources of Wayside Noise Generated by High-Speed Trains." *J. Sound Vib.*, 66, 311–332, 1979. doi:10.1016/0022-460X(79)90848-4.

[9] H.-M. Noh, S. Choi, S. Hong, and S.-W. Kim. "Investigation of noise sources in high-speed trains." *Proceedings of the Institution of Mechanical Engineers, Part F: Journal of Rail and Rapid Transit*, 228(3), 307–322, 2014. doi:10.1177/0954409712473095.

[10] F. Poisson. "Railway noise generated by high-speed trains." *Notes on Numerical Fluid Mechanics and Multidisciplinary Design*, 126, 457–480, 2015. doi:10.1007/978-3-662-44832-8_55.

[11] E. Sarradj, T. Geyer, H. Brick, K.-R. Kirchner, and T. Kohrs. "Application of beamforming and deconvolution techniques to aeroacoustic sources at highspeed trains." In *NOVEM - Noise and Vibration: Emerging Methods, Sorrento*. 2012.

[12] P. Sijtsma. "Phased array beamforming applied to wind tunnel and fly-over tests." In *SAE Brasil International Noise and Vibration Congress*. SAE International, 2010. ISSN 0148-7191. doi:https://doi.org/10.4271/2010-36-0514. URL https://doi.org/10.4271/2010-36-0514.

[13] D. Thompson, E. Latorre Iglesias, X. Liu, J. Zhu, and Z. Hu. "Recent developments in the prediction and control of aerodynamic noise from high-speed trains." *International Journal of Rail Transportation*, 3, 1–32, 2015. doi:10.1080/23248378.2015.1052996.

[14] J. Zhang, G. Squicciarini, and D. J. Thompson. "Implications of the directivity of railway noise sources for their quantification using conventional beamforming." *Journal of Sound and Vibration*, 459, 114841, 2019. ISSN 0022-460X. doi:https://doi.org/10.1016/j.jsv.2019.07.007. URL http://www.sciencedirect.com/science/article/pii/S0022460X19303955.

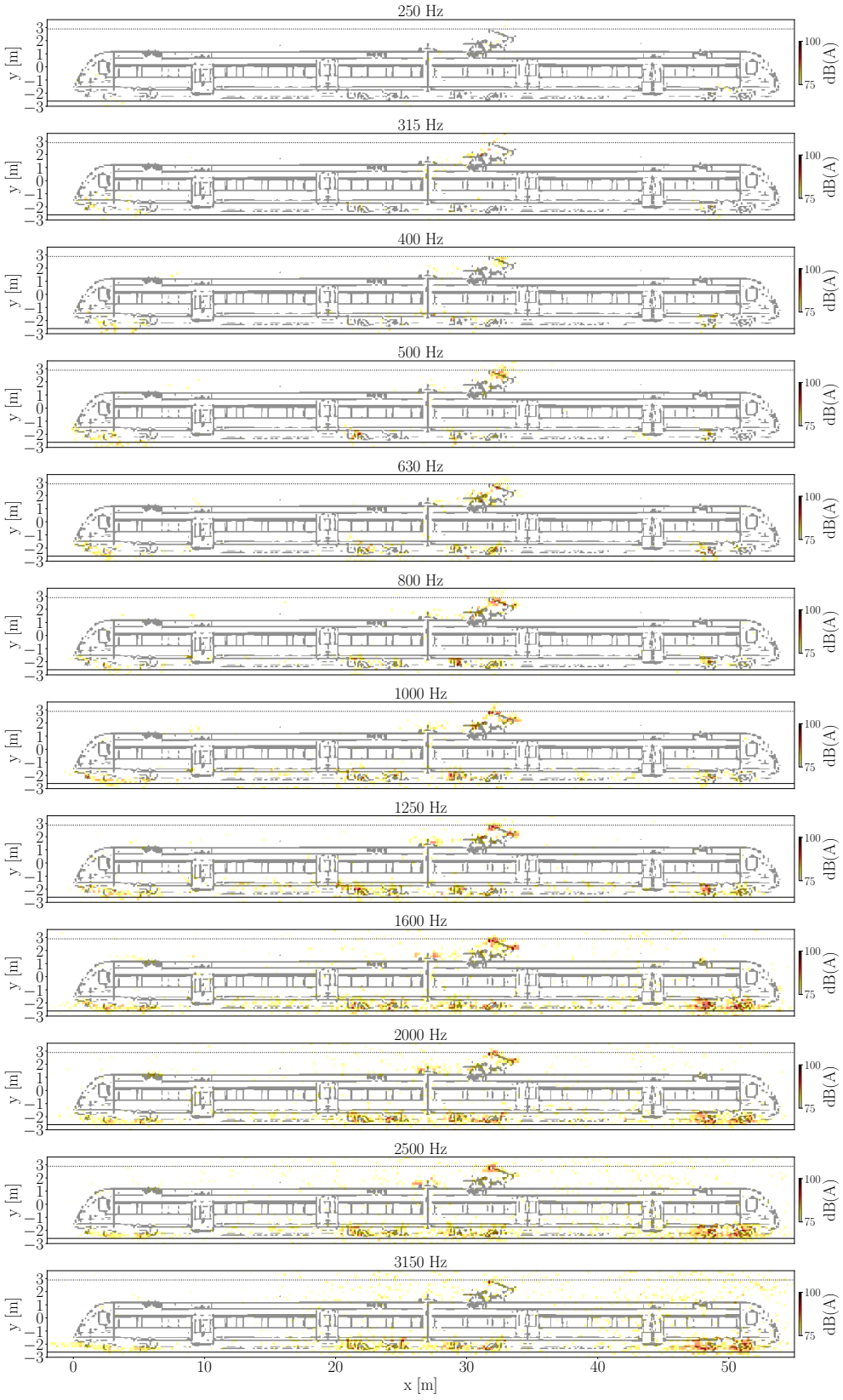

Figure 6: Deconvolved source maps for each of third octave band between 250 Hz and 3150 Hz, collected at Track A. ($\gamma = 0.6$, with diagonal deletion, A-weighted)

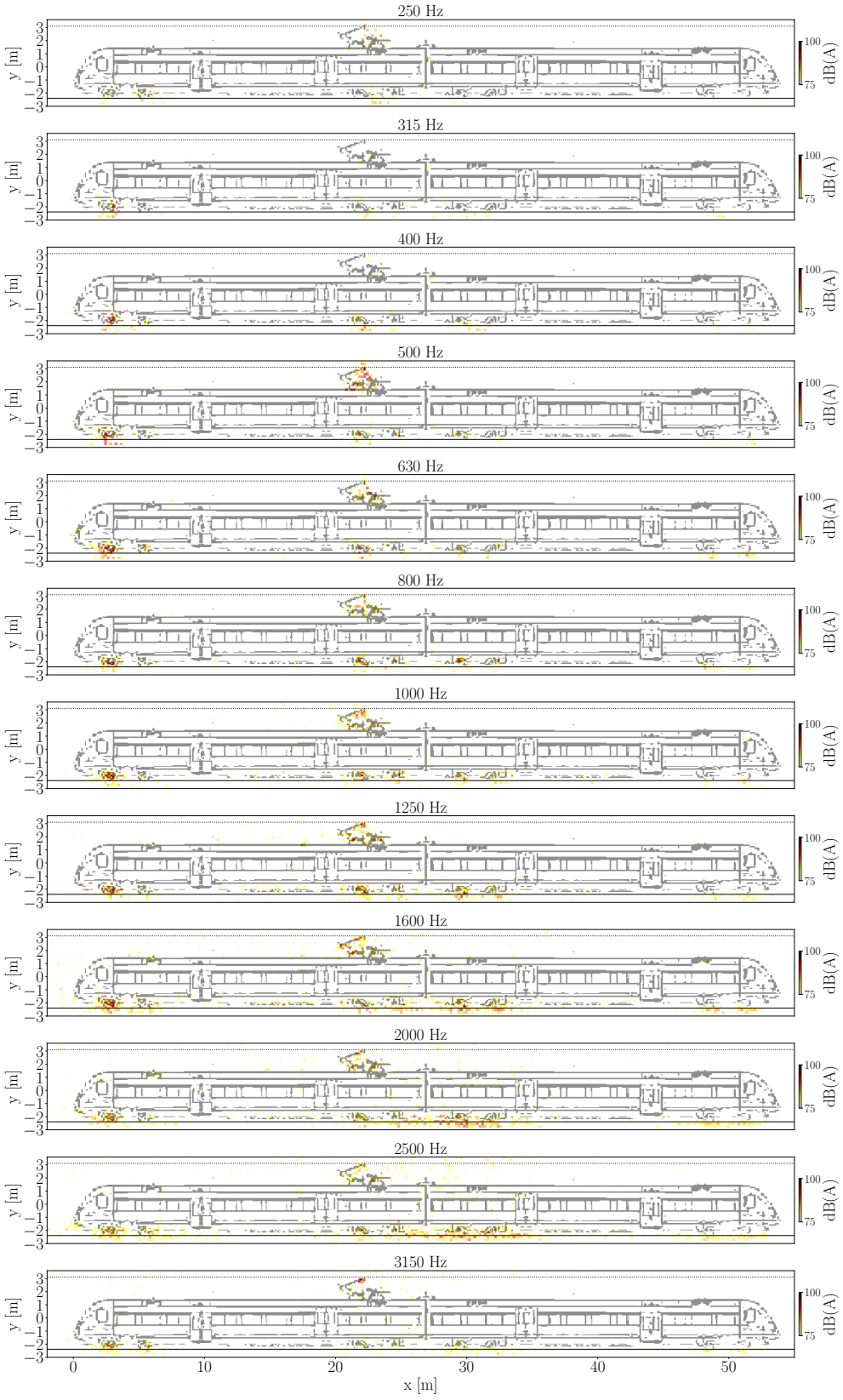

Figure 7: Deconvolved source maps for each of third octave band between 250 Hz and 3150 Hz, collected at Track B. ($\gamma = 0.6$, with diagonal deletion, A-weighted)